Proceedings in Manufacturing Systems, Volume 18, Issue 2, 2023, 51-59 ISSN 2067-9238

REAL TIME DATA ACQUISITION OF LOW-COST CURRENT SENSORS ACS712-05 AND INA219 USING RASPBERRY PI, DAQCPLATE AND NODE-RED

Adrian MAROȘAN[1,*], George CONSTANTIN[2], Claudia Emilia GÎRJOB[3], Anca Lucia CHICEA[4], Mihai CRENGANIȘ[5]

[1)] Asst. Prof., PhD, Machines and Industrial Equipment, University "Lucian Blaga" of Sibiu, Faculty of Engineering, Romania
[2)] PhD, Prof., Robots and Manufacturing Systems Department, University "Politehnica" of Bucharest, Romania
[3)] Assoc. Prof., PhD, Machines and Industrial Equipment, University "Lucian Blaga" of Sibiu, Faculty of Engineering, Romania
[4)] Assoc. Prof., PhD, Machines and Industrial Equipment, University "Lucian Blaga" of Sibiu, Faculty of Engineering, Romania
[5)] Lecturer, PhD, Machines and Industrial Equipment, University "Lucian Blaga" of Sibiu, Faculty of Engineering, Romania

Abstract: *Current monitoring is critical to ensuring the proper operation of equipment and mobile devices, providing vital information about battery health, range, and charge level. This study focuses on the use of two affordable sensors, ACS712-05 and INA 219, for real-time current monitoring. These sensors can be easily integrated into a variety of applications such as mobile robots, drones, or photovoltaic panels. To collect the data from these sensors, a Raspberry Pi minicomputer is used in combination with a DAQCplate data acquisition board. Custom models are developed in Node-RED, containing specific blocks for data acquisition of each sensor, to facilitate the current monitoring process. Analyzing the data obtained from these sensors, several important conclusions are made. These conclusions provide a deeper understanding of how current monitoring technologies can be implemented and highlight significant differences between the various approaches. The results of this study are especially valuable for the further development of mobile equipment or modular mobile robots. They provide essential clues for improving the performance and efficiency of these devices.*

Key words: *ACS712-05, INA219, Low-cost sensors, Raspberry Pi, DAQCplate, Node-RED, Mobile robots, Current monitoring.*

1. INTRODUCTION

Nowadays, climate change is a pre-eminent concern in global society, attracting attention for several decades. Currently, these concerns have intensified and put the emphasis on energy consumption in society. This debate has become even more complex in the context of the ever-expanding integration of technology and the development of solutions to automate most of the daily activities on which society increasingly depends. Specifically, embedded devices, such as those used in a variety of systems and equipment, including household appliances, or home heating systems, but also consumer electronics such as mobile phones, laptops, but also medical applications or car systems, such as those for collision avoidance, braking or fuel monitoring. All these devices are based on a software and a hardware system that consumes more and more energy. Additionally, the evolution of modern processors has continued to bring an increase in the number of transistors and components integrated into the same space, along with an increase in processor core frequencies. This advance has created a significant demand for energy and resources from modern computer systems [1]. Current information is essential in a wide range of electrical and electronic applications. Each application imposes specific requirements related to cost, isolation, accuracy, bandwidth, measurement range, or size, and to meet these requirements, multiple current measurement methods have been developed. Nowadays, there is a significant increase in the need for this information to be available in digital format to be used for digital control or monitoring purposes. This conversion to digital format requires an output signal generated by a specific current sensing technique, which will then be converted to digital format by an analog-to-digital converter. For example, shunt resistors have been widely used in power electronics due to their low cost, compact size, and relative simplicity while providing acceptable accuracy. However, as greater integration, increased efficiency, and the ability to implement more sophisticated control techniques are sought, analog control loops are gradually being replaced by digital ones. Consequently, the current data must go through a digitization process. It is also important to note that a small voltage drop across a shunt resistor requires amplification, which can affect signal bandwidth and increase device size and cost. As power converters have reached significant levels of power density, energy losses within shunt resistors are becoming increasingly problematic. Therefore, power electronics engineers are exploring alternatives that provide similar accuracy but minimize power losses and allow an output voltage that can be directly converted to digital format by an analog-to-digital converter [2].

[*] Corresponding author: Emil Cioran nr.4, Sibiu,Romania, Tel.: +40742945750.
E-mail addresses: *adrian.marosan@ulbsibiu.ro* (A. Maroșan), *george.constantin@icmas.eu* (G. Constantin)

2. LITERATURE REVIEW

After a careful review of the literature, it was noticed that there are numerous articles that present studies that have been performed using the ACS712 and INA219 current sensors. These articles explore the performance and applications of these sensors in depth, providing detailed insight into how they are used to measure current in a variety of contexts. These publications also highlight the advantages and limitations of each sensor and provide useful data for researchers and electronics and electrical professionals who wish to integrate these devices into their projects. The paper [3] details the manual assembly process of a monitoring network developed to collect current data from the ACS712 and ACS723 Hall Effect Current Sensors. The data is then transmitted via Bluetooth wireless technology to an Arduino platform. This information is then integrated into a graphical monitoring program, which works as an application on an Android smartphone. Originally designed to be implemented in the WALK-E GPS-based autonomous navigation system, this monitoring system could collect and view important current-related data, thus contributing to the efficient operation of the WALK-E device. The article [4] details the design and implementation of an off-grid photovoltaic energy management system with the objective of battery monitoring and energy estimation. Current monitoring is used to estimate the state of charge of a 24 V, 100 Ah lead-acid battery bank. The ACS712 module is used to implement current and energy consumption monitoring. Energy estimation is successfully achieved with a root mean square error of 6.2% for a continuous three-day test. It is concluded that the proposed solution successfully demonstrates a working principle for an energy management system, however, further improvements are needed to make the forecasting model as accurate as possible. Paper [5] presents a system that allows real-time monitoring of electricity consumption, using the ACS712 for current measurement and the ZMPT101B for voltage measurement, in combination with the Arduino platform and an Internet of Things (IoT) solution. This system can provide the user with information on electricity consumption expressed in kilowatt-hours (kWh) and the calculation of the associated costs for the electricity bill. The user interface for this system is available as an app for the Android platform. The current measurement error is reduced to less than 2%, and the peak-to-peak voltage measurement error is 4%. The system is also able to generate notifications to inform the user about the amount of electricity consumed or the costs associated with the consumption, thus providing increased transparency regarding the use of electricity. In another article, [6], a fast, portable, and economical measurement system is presented that is capable of accurately evaluating the basic electrical characteristics of electronic devices. This system is controlled by a MATLAB application that communicates with an Arduino Nano microcontroller, responsible for managing two AD5761 16-bit 20V digital-to-analog converters, as well as for current monitoring via a high-resolution INA219 shunt sensor. The raw data collected by the system is graphed in real time using MATLAB and is automatically recorded in a *.csv* file, including the date and time it was recorded. This approach allowed for results with a negligible difference compared to data collected using high-tech instruments such as a Keithley 2410 and a semiconductor B1500 for analysis. Therefore, the proposed system is an economical and efficient alternative to the advanced instruments used for current measurement. In the article [1] performs an analysis of the power consumption characteristics of a development board with a small form factor and highly competitive costs, namely the Raspberry Pi4 Model B. The evaluation focuses on the impact on power consumption when the development board operates with a minimal load, either in a bare-metal configuration or with a default operating system. Different levels of processing frequency scaling (underclocking) and the corresponding effect on core power consumption are also considered. The experimental setup involves using a current sense amplifier, such as the INA219, to record power, current, and voltage measurements, along with a Teensy 4.0 microcontroller for data collection. The results obtained indicate statistically significant differences in terms of total energy consumption, as well as significant variations in its distribution in all tested models. Additionally, the results indicate the existence of three distinct power consumption zones depending on the underclocking frequency levels and bare-metal configurations. There are also statistically significant differences in both the mean and median power measurements between the various underclocking frequency test scenarios and bare-metal configurations. In conclusion, the results suggest that power consumption is a monotonically increasing function in different test scenarios. It is also noted that isolating the power consumption into separate distributions increases the predictability of the model from 67% to 97%. Article [7] discusses a research dedicated to the measurement of solar energy harvesting in the region of Indonesia, using an ATmega328P microprocessor logger and an INA219 current sensor module. The purpose of this research is to evaluate the performance of an autonomous photovoltaic system. In this assessment, the measured variables include solar radiation, voltage, current, power, energy, and temperature. The research methodology involves comparing the results obtained within the photovoltaic system with maximum power point tracking technology (MPPT) with those of a system without MPPT technology. In addition, the solar irradiance measurement using the solar energy meter is compared with solar irradiance data provided by NASA. The obtained results highlight an improvement in the performance of the photovoltaic system with MPPT compared to the system without this technology, and the most efficient photovoltaic system with MPPT technology obtained a performance ratio (PR) of 0.93.

2.1. Research objectives

After reviewing the available articles, a need was identified for a paper that provides a real-time current monitoring solution using sensors that are affordable and easy to implement in a variety of applications. This solution would be beneficial from both an educational

and a research perspective. Thus, the paper proposes a method of current monitoring with the help of ACS712 and INA 219 sensors, using a Raspberry Pi mini computer.

3. MATERIALS AND METHODS

3.1. Current sensors ACS712 and INA219

Hall sensors are used in a variety of applications, such as photovoltaic panels, induction motors, wind turbines and DC motors, to measure electric current. The operating principle is based on the passage of the electric current, denoted by *I*, through a magnetic field, which leads to the generation of a voltage proportional to the density of the magnetic field. The working mechanism of the Hall effect sensor is based on the Lorentz force, as illustrated in Fig. 1. When the magnetic field *B* (representing the magnetic flux density) penetrates a metal plate perpendicularly, a deformation force known as the Lorentz force occurs, expressed as $F = q(v \times B)$, where q represents the electric charge and v represents the particle velocity. This force generates a deflection of the charge in a direction perpendicular to both the direction of the current I and the direction of the magnetic field *B*, thus resulting in a voltage denoted by *v*, which is perpendicular to both the current *I* and the magnetic field *B*. The expression of this electric tension is given by the relation:

$$v = IB / (nqd), \quad (1)$$

where: *q* – carrier charge, *n* – carrier density and *d* – sheet thickness.

For materials used in Hall sensors, such as indium antimonide (InSb), indium arsenide (InAs), and gallium arsenide (GaAs), the properties of these materials are summarized in the Hall coefficient:

$$RH = 1 / (nq). \quad (2)$$

The ACS712 sensor, which is based on the principle of the Hall effect, is integrated into the electrical system of the drive wheel module. Figure 2 shows a schematic of the ACS712 sensor, which includes an integrated circuit developed by Allegro. This current sensor has a linear behavior and can measure both direct current and alternating current. The manufacturer offers the sensor in three construction variants with different nominal values (±5 A, ±20 A and ±30 A). Table 1 provides details about each sensor variant, while Table 2 shows the main characteristics of this type of sensor [7].

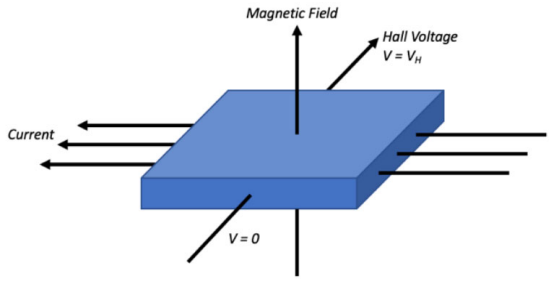

Fig. 1. Hall effect in a thin sheet of conductive material [7].

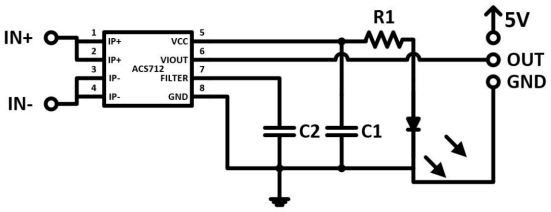

Fig. 2. Current sensor wiring diagram [7].

Table 1

Constructive variants of the ACS712 sensor [7]

Sensor model	Temperature (° C)	Measurement range	Sensitivity (mV/A)
ACS712005A	−40…85	±5	185
ACS712020A	−40…85	±20	100
ACS712030A	−40…85	±30	66

Table 2

Main features of the ACS712 sensor [7]

Parameters	Values
Minimum Isolation Voltage (Input and Output)	2.1 kVrms
Working Temperature	From (−40 la + 85) °C
Supply Voltage	5 V
Sensitivity (±5, ±20 and ±30) A	(66, 100, 185) mV/A
Drawn current	10 mA

To perform the current measurements, a bidirectional sensor named ACS712ELCTR-05A model was used, whose characteristic curve is shown in Fig. 3. This curve shows that the output voltage of the sensor is fixed at 2.5 V, and at this value, the theoretical current should be zero. However, in practice, the value of 0 A is not reached due to various interferences from multiple sources, such as the influence of other magnetic fields, noise, etc. For this sensor model, the sensitivity is 185 mV/A, and if the output voltage is below 2.5 V, then the current value is negative [7].

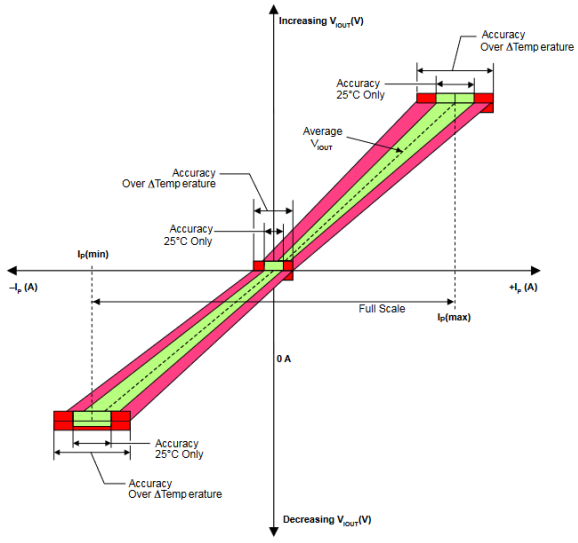

Fig. 3. Operating curve of the current sensor [7].

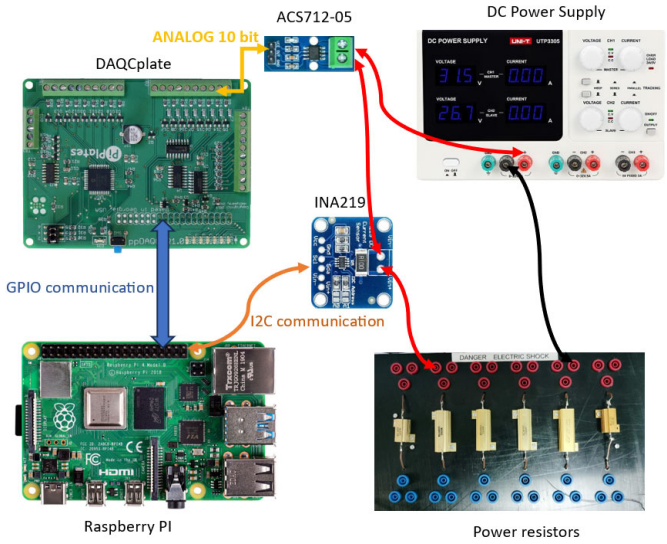

Fig. 4. Hardware configuration for current measurement.

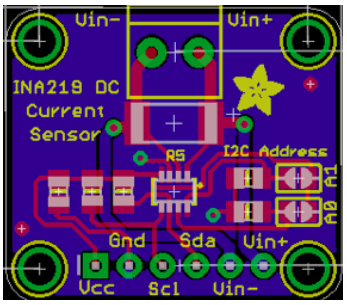

Fig. 5. INA219 current sensor [1].

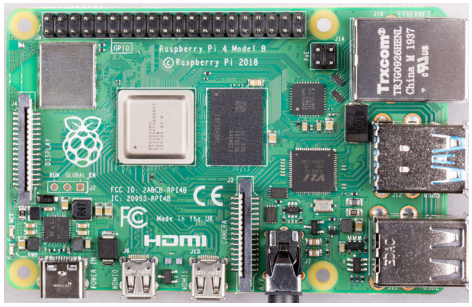

Fig. 6. Raspberry Pi 4 Model [1].

The INA219 sensor is equipped with a precision amplifier that measures the voltage drop across a sense resistor with a nominal power of 0.1 W, specifying an error of only 1%. The maximum voltage difference that the amplifier can measure is 320 mV, and this sensor can measure currents up to 3.2 A. To make these measurements, an internal analog-to-digital converter (ADC) is used with a 12-bit resolution, thus ensuring an accuracy of 0.8 mA. Figure 5 shows a graphical representation of the sensor and indicates pins such as VCC, GND, SCL, SDA, Vin and Vin+ as inputs and outputs, while VCC and GND provide power and SCL and SDA are the pins used for I2C communication, facilitating data transfer between sensor and microcontroller.

3.2. Raspberry Pi 4 Model B and DAQCplate

To acquire real-time data, a Raspberry Pi 4 Model B mini-computer (developed by Raspberry Pi (Trading) Limited, based in Cambridge, United Kingdom) was used. It integrates a Broadcom BCM2711 processor with four Cortex-A72 cores (ARM v8), operating on a 64-bit architecture. The processor has a main reference clock speed of 1.5 GHz. Raspberry Pi has 32 KB of data memory, 48 KB of L1 instruction cache per core, 1 MB of L2 cache, and 4 GB of LPDDR4-3200 SDRAM.

For network connectivity, Raspberry Pi is equipped with IEEE 802.11ac wireless interfaces at 2.4 GHz and 5.0 GHz, Bluetooth 5.0, 2 USB 3.0 ports, and 2 USB 2.0 ports. It also provides general-purpose input-output (GPIO) functionality through a 40-pin GPIO header. Raspberry Pi can be powered either via a 5 V DC USB-C connector or through the GPIO headers with 5 V DC. The maximum tolerated current is 3 Amperes. For more details, you can refer to the specifications diagram presented in Fig. 6.

Due to the absence of dedicated GPIO pins for analog inputs and outputs on the Raspberry Pi mini-computer, the use of an additional acquisition board or specialized boards equipped with analog-to-digital converters (ADC) is necessary. For this project, we chose to employ a specially developed board designed for the Raspberry Pi, known as the DAQCplate, as illustrated in Fig. 7. This board was selected for its capability to enhance the Raspberry Pi's performance in the realm of analog data acquisition. The primary features of this acquisition board are detailed in Table 3, in accordance with the technical documentation provided by the manufacturer on its website. By utilizing the DAQCplate, we were able to transform the Raspberry Pi into a more versatile data acquisition instrument, capable of measuring analog signals and converting them into a digital format for subsequent processing. This solution significantly expanded our capacity to collect and analyse data within the project.

Fig. 7. DAQCplate.

Table 3

Main features of Pi-Plates DAQCplate [8]

Parameters	Description
Analog Inputs	Eight protected inputs 0 to 4.096 V input range 10-bit resolution. Dedicated channel for measuring power supply voltage.
Analog Outputs	Two protected outputs 0 to 4.096 V output range 10-bit resolution
Digital Inputs	8 protected inputs, 3.3 and 5.0 logic compatible. Each input capable of reading a DS18B20 temperature sensor. Can be polled or programmed to generate an interrupt on change.
Open Collector Outputs	7 Outputs, Indicator LEDs on each output, 350mA sink current for each channel. Built in flyback current protection. Maximum load voltage of 12 VDC.
Pulse Width Modulators	Two protected independent outputs 10 bits of resolution. Resource shared with Analog Outputs.

Figure 8 illustrates the essential hardware connections to perform real-time current measurements using the two mentioned sensors. In this image, one also notice a board equipped with several power resistors, used to evaluate the current drawn by various circuit configurations that were built using these components. In addition, in the same figure, one can identify a UNI-T UTP3305 laboratory power supply, which has three channels. Two of these channels allow the supply of a variable voltage in the range of 0 to 32 V and a current of 5 A, while the third channel provides a fixed voltage of 5 V and a current of 3 A. This complex hardware setup is essential to collect data as accurately as possible to power the circuits correctly during current measurements. Figure 8 shows a board that houses several types of power resistors. This image shows the existence of 6 power resistors, thus providing a wide range of options for building circuits designed to absorb a specific current.

The parameters of these power resistors are detailed in Table 4, providing information such as the resistors' nominal value, measured value, tolerance, and related power. This arrangement of power resistors provides important versatility in current measurement projects, allowing the precise selection and configuration of the resistors needed to meet the specific requirements of different applications. Table 4 provides essential details for choosing the correct resistors and ensuring an accurate and current measurement.

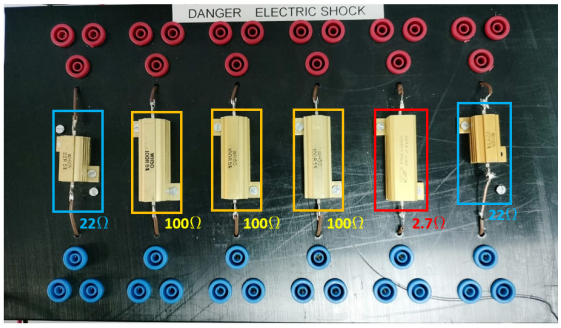

Fig. 8. Power resistors for current measurement.

Table 4

Power resistor plate parameters

Nominal value	Measured value	Tolerance	Power	Quantity
100 Ω	99.5 Ω	±5%	50 W	3
22 Ω	21.96 Ω	±5%	25 W	2
2.7 Ω	2.78 Ω	±5%	50 W	1

3.3. Simulation and measurement of the current absorbed by the power resistors

To measure the current absorbed by the available power resistors, an electrical circuit simulation program was used first. With the help of this simulation software, a series of 5 configurations was performed. The first configuration is shown in Figure 9 where the 99.5 Ω resistor is connected to a voltage of 12 V, resulting in a current of 121 mA.

As for configuration 2, it was decided to use a resistor with a value of 21.96 Ω, and this was also supplied with a voltage of 12 volts. According to the simulation results, the current in this circuit was 548 mA. This can also be seen in Fig. 10, which shows the simulation and the current value.

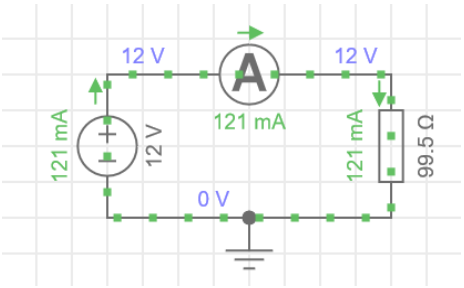

Fig. 9. Configuration 1 current simulated 121 mA.

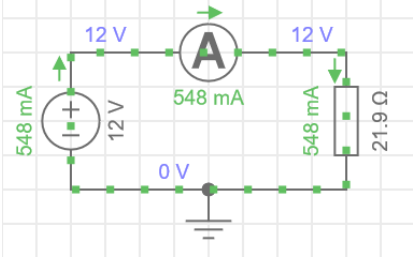

Fig. 10. Configuration 2 current simulated 548 mA.

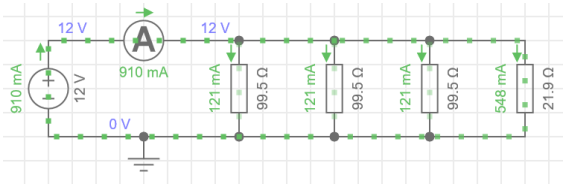

Fig. 11. Configuration 3 current simulated 910 mA.

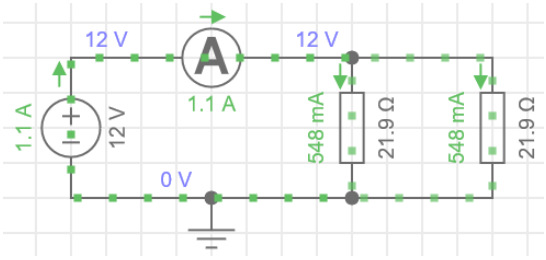

Fig. 12. Configuration 4 current simulated 1100 mA.

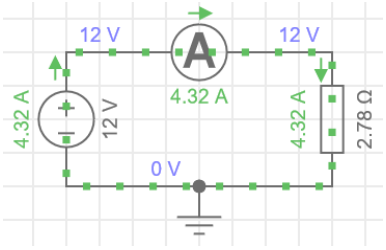

Fig. 13. Configuration 5 current simulated 4320 mA.

For configuration 3, an approach was taken where we used 4 power resistors connected in parallel, all powered at 12 volts. In this configuration, 99.5 Ω resistors and 1 21.9 Ω resistor were used. According to the simulations, the current in this circuit was 910 mA. This configuration involved the use of a mixture of resistors of different values, strategically connected in parallel to obtain a specific current. This aspect can be seen in detail in Fig. 11, which shows the circuit diagram.

Configuration 4 shows a circuit with 2 resistors connected in parallel, both having values of 21.9 Ω. And in the case of this configuration, the supply voltage was also 12 V. Following the simulation according to Fig. 12, the current in this circuit is 1.1 A.

The last configuration shows the connection of a power resistor with a value of 2.78 Ω at a voltage of 12 V. According to the program used to simulate the current absorbed by the power resistor, in this case it is obtained a current of 4.32 A. This is also visible on the diagram resulting from the simulation illustrated in Fig. 13.

EveryCircuit software was used to simulate the current drawn by the power resistors. EveryCircuit is a circuit simulation application that allows users to design and simulate electronic circuits on their mobile devices or personal computers. This application provides an interactive and intuitive interface, allowing users to experiment with various electronic components and understand the behavior of circuits in a virtual environment. The real-time current measurement was performed using the mentioned components according to Fig. 4. The data acquisition interface was implemented in the Node-RED application, which runs on the Raspbian operating system. Node-RED is an open-source platform for visual application development, specialized in creating data flows (flow-based programming). This platform is used to connect devices and services in an accessible and intuitive way, allowing developers to quickly create IoT (Internet of Things) applications, automations, and integrations between various systems.

To measure analogue signals in a digital computing system, they must be converted into discrete numerical values. The important feature of an ADC is its resolution, which is the number of discrete values at the output of the converter in a measurement range. These values are stored in binary form and for this reason the resolution of an ADC is expressed in bits. The DAQC plate's ADC has a resolution of 10 bits, which means it can provide 2^{10} = 1024 different output values. If the measurement range is from 0 to 5 V, then the measurement resolution will be:

$$K_u = U_a / r_e, \tag{3}$$

where K_u – the voltage value at the output of the analog-to-digital converter (ADC), U_a – the analog voltage measurement range and r_e – the ADC resolution.

$$K_u = 5\text{V} / 1024 \Rightarrow K_u = 4.88 \text{ mV}. \tag{4}$$

To monitor the current using the ACS712ELCTR-05A sensor, the characteristic curve in Fig. 3 must be considered, which shows that the output voltage of the sensor is equal to 2.5 V, and for this value, the theoretical current is 0 A. The calculation relationship used to determine the current is as follows:

$$I = (V_{sc} - K_v) / S_s, \tag{5}$$

where I – electric current intensity, Vsc – voltage sensor calibration, Kv – sensor constant of 2.5 V for I = 0 A and Ss – sensor sensitivity (according to data sheet, 185 mV/A). In practice, however, the value of 0 A does not exist, because there are variations caused by several causes, such as interference with other magnetic fields, noises, etc. Because of this, the value of the voltage supplied by the ADC of the acquisition board is highly variable. To smooth out these voltage spikes, voltage sensor calibration (Vsc) is used. The sensor calibration block was used, as illustrated in Fig. 14. The blue chase represents a low pass filter and, the voltage Ku is read 10 times at various intervals and entered a summation block. At the output of the block, an arithmetic mean is calculated and multiplied by the constant Kc = 1/10. With this solution, voltage fluctuations are still present, but their variation is smaller. In the case of the INA219 sensor, it is eliminated the need to use signal calibration blocks in Node-RED, as there is a specialized block within this environment for managing this type of sensor.

Thus, the measured quantity is the current, in milliamperes (mA), as illustrated in Fig. 15. Since the sensor communicates via the I2C protocol with the Raspberry Pi, no additional acquisition board is required. This not only simplifies the system setup, but also helps reduce the cost and complexity of the overall measurement system. In addition, the resolution of the signal measured by the sensor is 12 bits, ensuring significant accuracy in detecting and recording current variations.

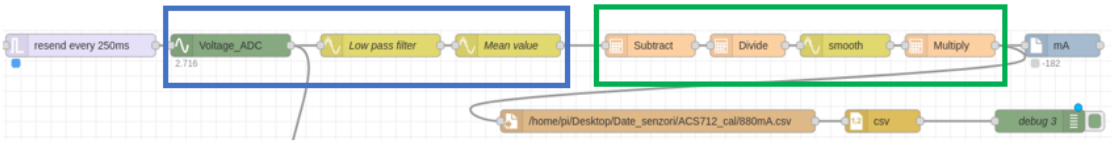

Fig. 14. Node-RED data flows ACS712.

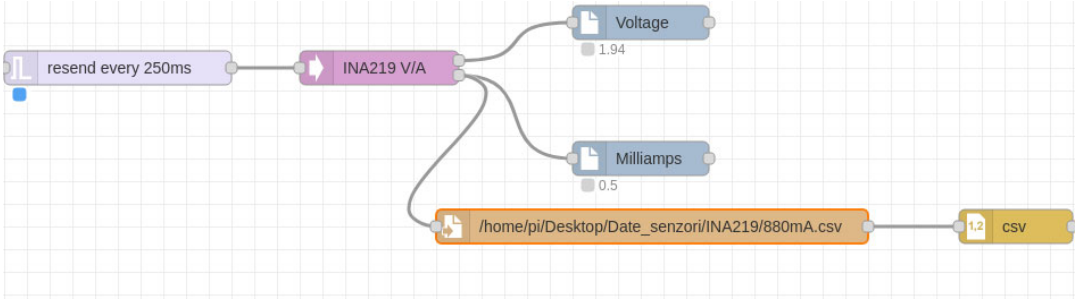

Fig. 15. Node-RED data flows INA219.

4. RESULTS

The experiments were carried out using the stand shown in Fig. 16, where the image of the experimental research can be seen. All five configurations were successfully implemented using this stand, initially simulated using EveryCircuit software.

Table 5 shows the data obtained for the 121 mA configuration shown in Fig. 17. In this figure, the graph for the simulated current, the current acquired from the INA 219 sensor and the current acquired from the ACS712-05 sensor can be seen. According to Table 5, it can be seen that the average current value for the

Table 5

Results of measured current (121 mA)

		Simulated current	Error
Current INA219	122.4 mA	121 mA	1.15%
Current ACS712	103 mA	121 mA	14.8%
Error	15.8%		

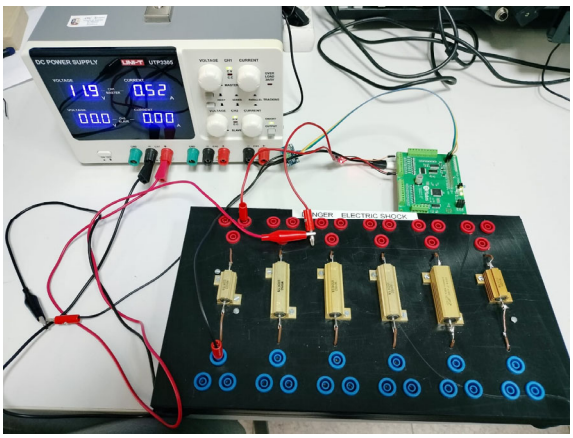

Fig. 16. Imagine of the experimental stand.

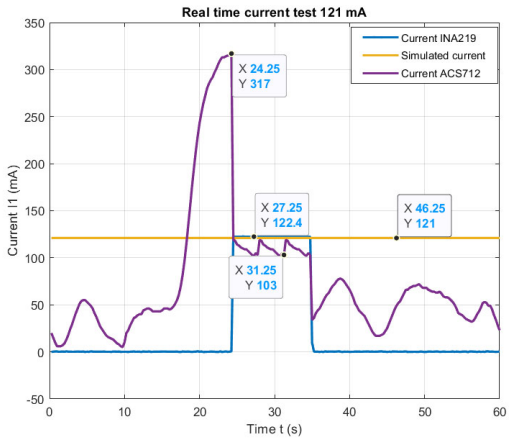

Fig. 17. Configuration 1 (measured current 121 mA).

INA219 sensor is 122.4 mA, resulting in a relative error between the measured and simulated current of 1.15%. For the ACS712-05 sensor, the average current value is 103 mA, resulting in a relative error between simulated and measured current of 14.8%. It can also be seen that the relative error between the two sensors is 15.8%.

Table 6 shows the data obtained for the 548 mA configuration shown in Fig. 18. In this image, the graph for the simulated current, the current acquired from the INA 219 sensor and the current acquired from the ACS712-05 sensor can be seen.

According to Table 6, the average current value for the INA219 sensor is 550.5 mA, resulting in a relative error between the measured and simulated current of 0.45%. In the case of the ACS712-05 sensor, the average value of the current is 502 mA, resulting in a relative error between the simulated and measured current of 8.39%. It can also be seen that the relative error between the two sensors is 8.81%.

Table 7 shows the data obtained for the 910 mA configuration shown in Fig. 19. In this image, the graph for the simulated current, the current acquired from the INA 219 sensor and the current acquired from the ACS712-05 sensor can be seen. According to Table 7, it

Table 6

Results of measured current (548 mA)

		Simulated current	Error
Current INA219	550.5 mA	548 mA	0.45%
Current ACS712	502 mA	548 mA	8.39%
Error	8.81%		

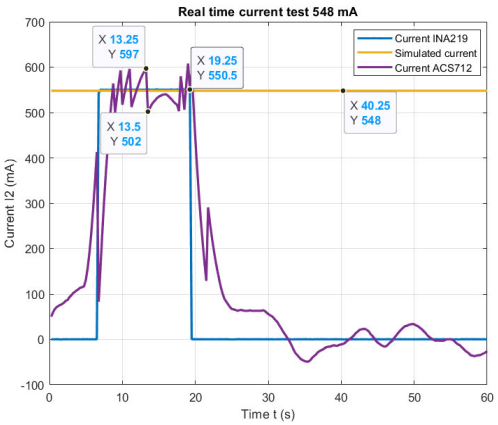

Fig. 18. Configuration 2 (measured current 548 mA).

Table 7

Results of measured current (910 mA)

		Simulated current	Error
Current INA219	903.4 mA	910 mA	0.72%
Current ACS712	976 mA	910 mA	6.76%
Error	7.43%		

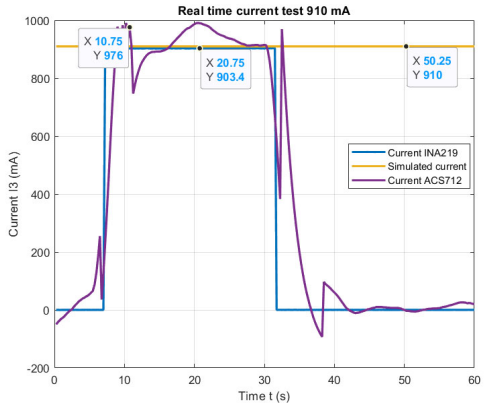

Fig. 19. Configuration 3 (measured current 910 mA).

can be seen that the average current value for the INA219 sensor is 903.4 mA, resulting in a relative error between the measured and simulated current of 0.72%. In the case of the ACS712-05 sensor, the average current value is 976 mA, resulting in a relative error between the simulated and measured current of 6.76%. It can also be seen that the relative error between the two sensors is 7.43%.

Table 8

Results of measured current (1100 mA)

		Simulated current	Error
Current INA219	1082.1 mA	1100 mA	1.62%
Current ACS712	1050 mA	1100 mA	4.54%
Error	2.96%		

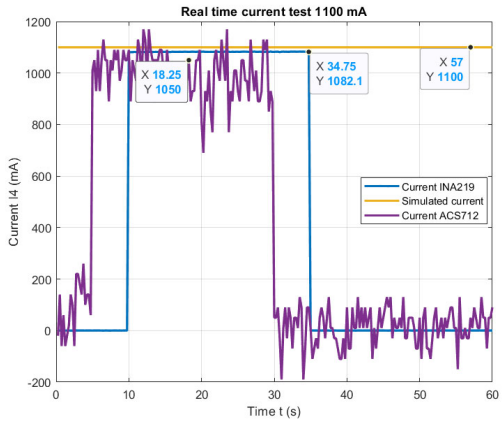

Fig. 20. Configuration 4 (measured current 1100 mA).

Table 8 shows the data obtained for the 1100 mA configuration shown in Fig. 20. In this image, the graph for the simulated current, the current acquired from the INA 219 sensor and the current acquired from the ACS712-05 sensor can be seen.

According to Table 8, it can be seen that the average current value for the INA219 sensor is 108.21 mA, resulting in a relative error between the measured and simulated current of 1.62%. In the case of the ACS712-05 sensor, the average value of the current is 1050 mA, resulting in a relative error between the simulated and the measured current of 4.54%. It can also be seen that the relative error between the two sensors is 2.96%.

Table 9 shows the data obtained for the 4320 mA configuration shown in Fig. 21. In this image, one can see the graph for the simulated current, the current acquired from the INA 219 sensor and the current acquired from the ACS712-05 sensor. According to Table 9, it can be seen that the average current value for the INA219 sensor is 3200 mA, resulting in a relative error between the measured and simulated current of 25.9%. It is important to specify that the measurement range for the INA219 sensor according to the technical sheet is between 0 - 3.2 A, due to this fact, the value of the relative error is high. In the case of the ACS712-05

Table 9

Results of measured current (3200 mA)

		Simulated current	Error
Current INA219	3200 mA	4320 mA	25.9%
Current ACS712	4070 mA	4320 mA	5.78%
Error	27.18%		

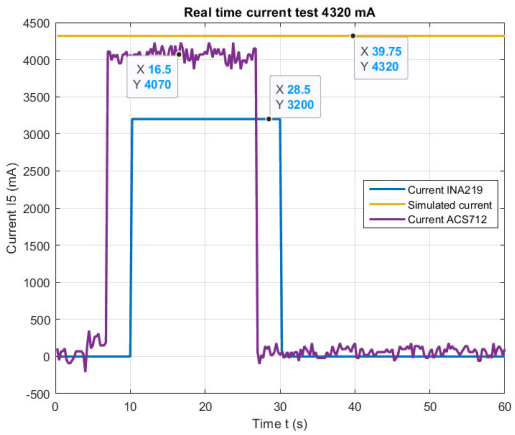

Fig. 20. Configuration 5 (measured current 4320 mA).

sensor, the average value of the current is 4070 mA, resulting in a relative error between the simulated and the measured current of 5.78%. It can also be seen that the relative error between the two sensors is 27.18%.

5. CONCLUSIONS

Following the experimental validation, the presence of small discrepancies between the simulated current and the one measured in real time is highlighted. In the context of the ACS712 sensor, it is found that the maximum error value between the simulated and the measured current reaches 14.8% for the 121 mA configuration. The lowest degree of error was recorded in the case of the 1100 mA configuration, with a value of only 4.54%. Regarding the INA219 sensor, the maximum error between simulated and measured current was 1.62% in the 1100 mA configuration, and the smallest error was 0.45% in the 0.45% configuration. According to the technical specifications of the INA219 sensor, it can detect a bidirectional current of maximum 3200 mA. However, in the case of the 4320 mA configuration, a significant error of 25.9% is found between the simulated and measured current. The conclusion derived from these results indicates that the INA219 sensor is more accurate than the ACS712 sensor. However, for measuring currents higher than 3.2A, it is necessary to use a different model than the one presented in this paper. The model presented in the NODE-Red interface represents an effective solution for real-time current monitoring in various applications, using both hardware components and the proposed methods. Following this experimental validation, it is found that these sensors can be used at a low cost, although they have some limitations. In addition, the methods and components presented in this paper constitute a solid basis for new research directions. Based on these results, future research directions aim to develop new current monitoring methods using other sensors and acquisition boards with higher resolutions. In addition, the integration of these methods is aimed at monitoring the energy consumption of autonomous mobile robots or industrial equipment.

Acknowledgements: This research was funded by Lucian Blaga University of Sibiu (Knowledge Transfer Center) & Hasso Plattner Foundation research grants LBUS-HPI-ERG-2023, grant LBUS-HPI-ERG-2023-02.

REFERENCES

[1] J. Lambert, R. Monahan, and K. Casey, *Power Consumption Profiling of a Lightweight Development Board: Sensing with the INA219 and Teensy 4.0 Microcontroller*, ELECTRONICS, vol. 10, no. 7, Apr. 2021, doi: 10.3390/electronics10070775.

[2] S. Ziegler, R. C. Woodward, H. H.-C. Iu, and L. J. Borle, *Current sensing techniques: A review*, IEEE Sens. J., vol. 9, no. 4, pp. 354–376, 2009.

[3] J. Romero-Perigault, W. Flores-Fuentes, K.-H. Jo, and D. Caceres Hernandez, *Wireless Current Monitoring for Autonomous Robot Navigation*, in 2019 IEEE 28TH INTERNATIONAL SYMPOSIUM ON INDUSTRIAL ELECTRONICS (ISIE), 2019, pp. 1717–1722.

[4] S. Nair, W. B. Gonzalez, and J. Braid, *Battery Monitoring and Energy Forecasting for an Off-Grid Solar Photovoltaic Installation*, in Proceedings – 2019 Southern African Universities Power Engineering Conference/Robotics and Mechatronics/Pattern Recognition Association of South Africa, SAUPEC/RobMech/PRASA 2019, 2019, pp. 697–702, doi: 10.1109/RoboMech.2019.8704728.

[5] N.M. Yoeseph, M. A. Safi'Ie, and F. A. Purnomo, *Smart Energy Meter based on Arduino and Internet of Things*, *IOP Conf. Ser,* Mater. Sci. Eng., vol. 578, no. 1, p. 012085, Sep. 2019, doi: 10.1088/1757-899X/578/1/012085.

[6] L.J. Bradley and N.G. Wright,*"Electrical Measurements and Parameter Extraction of Commercial Devices Through an Automated MATLAB-Arduino System*, IEEE Trans. Instrum. Meas., vol. 70, 2021, doi: 10.1109/TIM.2021.3104041.

[7] G. Constantin *et al.*, *Monitoring the Current Provided by a Hall Sensor Integrated in a Drive Wheel Module of a Mobile Robot*, Machines, vol. 11, no. 3, p. 385, 2023.

[8] https://pi-plates.com/product/daqcplate/ (Accessed on 08 November 2023).